THE JOURNAL OF PHYSICAL CHEMISTRY Letters

Letter

pubs.acs.org/JPCL

Detection of Multiconfigurational States of Hydrogen-Passivated Silicene Nanoclusters

Ricardo Pablo-Pedro,[†,∥] Hector Lopez-Rios,[‡,∥] Serguei Fomine,[*,‡] and Mildred S. Dresselhaus[§]

[†]Department of Chemistry, Massachusetts Institute of Technology, 77 Massachusetts Avenue, Cambridge, Massachusetts 02139, United States

[‡]Instituto de Investigaciones en Materiales, Universidad Nacional Autónoma de México, Apartado Postal 70-360, CU, Coyoacán, Ciudad de México 04510, Mexico

[§]Department of Physics and Department of Electrical Engineering and Computer Science, Massachusetts Institute of Technology, Cambridge, Massachusetts 02139, United States

Supporting Information

ABSTRACT: Utilizing density functional theory (DFT) and a complete active space self-consistent field (CASSCF) approach,we study the electronic properties of rectangular silicene nano clusters with hydrogen passivated edges denoted by H-SiNCs (n_z,n_a), with n_z and n_a representing the zigzag and armchair directions, respectively. The results show that in the n_z direction, the H-SiNCs prefer to be in a singlet (S = 0) ground state for $n_z > n_a$. However, a transition from a singlet (S = 0) to a triplet (S = 1) ground state is revealed for $n_a > n_z$. Through the calculated Raman spectrum, the S = 0 and S = 1 ground states can be observed by the E_{2g} (G) and A (D) Raman modes. Furthermore, H-SiNC clusters are shown to have HOMO−LUMO (HL) energy gaps, which decrease as a function of n_a and n_z for S = 0 and S = 1 states. The H-SiNC with a S = 1 ground state can be potentially used for silicene-based spintronic devices.

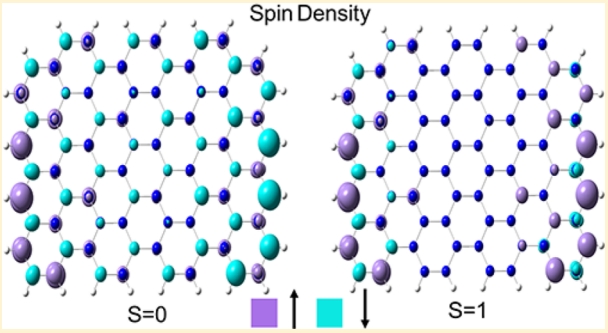

Although silicene was first theoretically predicted to be stable in nature by using first-principles calculations,[1,2] it was not until the actual synthesis of silicene in a lab[3−5] that stimulated the start of intense research of this material due to its similarities with graphene. Silicene is composed of Si atoms with a honeycomb structure like graphene, but with a buckled hexagonal layered structure composed of two sublattices, which are on different planes normal to the plane shown in Figure 1. As in graphene, the valence and conduction bands of silicene meet at two inequivalent Dirac points (K and K′ points) at the Fermi level.[2] This peculiar band structure gives rise to its exceptionally high electrical and thermal conductivities,[6] and also to many other interesting properties, such as the quantum spin Hall effect due to its additional spin−orbit coupling[7] compared to graphene. However, even though there is already conclusive experimental evidence for silicene formation upon different types of substrates,[5,8,9] the inherent difficulty of its synthesis has imposed constraints in obtaining free-standing silicene in the laboratory and in understanding the influences of doping, external fields, defects, and magnetic moments on the properties of this material, thereby limiting silicenes's exploitation in nanoelectronics and high-efficiency thermoelectric materials.[6,10,11]

Currently, most of the research has been done using theoretical and computational approaches, such as tight-binding models,[12] density functional theory (DFT),[13] and diffusion quantum Monte Carlo (DQMC) calculations.[14,15] Such approaches have indeed resulted in better understanding of

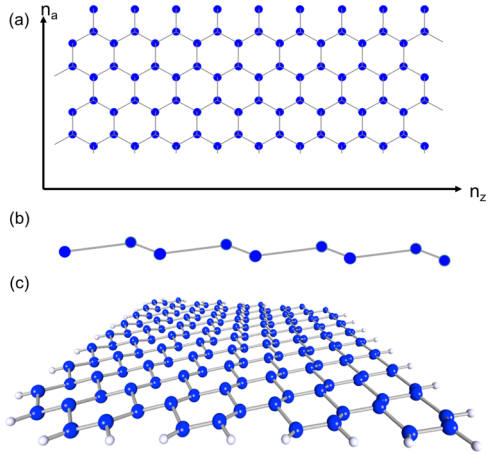

Figure 1. Top (a) and side (b) views of silicene, and (c) the optimized 3D geometry of an H-SiNC(8,8) structure, where the edges are passivated with hydrogen at the DFT (B3LYP) level of calculation.

Received: November 27, 2016
Accepted: January 16, 2017
Published: January 16, 2017

DOI: 10.1021/acs.jpclett.6b02773
J. Phys. Chem. Lett. 2017, 8, 615−620

the effect of increased spin−orbit coupling,[16] the increased interlayer binding energy in layered materials, the presence of the quantum spin Hall effect,[7] and the possibility of exploring topological phases of silicene under an external field perpendicular to the silicene layers.[17] However, until now, most of the theoretical findings reported for silicene have been done using the DFT level of theory with the generalized gradient approximation (GGA) functionals, local density approximation (LDA) functionals, and plane wave bases, none of which fully account for the electron-correlation. Therefore, only computational approaches that involve full configuration interaction (CI) and are based on multireference wave functions are capable of predicting the peculiarities of the silicene electronic behavior, such as in large conjugated systems that potentially possess multiconfigurational ground states.[18−20] Thus, the most frequently used method to treat electron correlation is known as a complete active space self-consistent field (CASSCF) approach.[21] However, the CASSCF calculation method is limited by the size of the system due to the huge number of available configurations that can be generated in the active space of the system. The latter issue is why using single-determinant approaches with an unrestricted formalism for the wave function construction turn out to be an alternative approach that is useful for large systems.

The application of single-determinant methods along with an unrestricted formalism for the wave function allows us to take the electrons' spin into account, but the results are often qualitatively poor, and the wave function is no longer an eigenfunction of the spin operator $\widehat{S^2}$. Therefore, the solutions thus obtained are spin-mixed, which is also known as spin-contamination. In many cases, the spin contamination from higher spin, i.e., $S = 1$ or $S = 2$, is quite negligible,[22] but for systems with unpaired electrons, such as graphene and silicene, the spin contamination could be quite significant.[23] So, higher spin states such as $S = 1$ could lead to nontrivial electronic properties. For example, it has been observed that the Berry's phase that typically encloses the Dirac point of $S = 1$ can vanish, leaving the Dirac point energetically isolated.[24−26] The emergence of a flat structure under this isolated Dirac point further indicates the presence of non-negligible electron correlation in these systems.[27] Additionally, systems with $S = 1$ can be potentially applied to spintronics.[28] Therefore, the problem of determining whether or not silicene possesses a multiconfigurational character and how to take electron correlation into account should be considered.

In this article we investigate the electronic properties of H-SiNCs, and the effect of electron correlation in H-SiNCs using multireferential first principals calculations that have not been done yet until now in DFT publications concerning silicene. For this study, we chose the pairing Beck 3-Parameter (exchange), Lee, Yang and Parr (B3LYP) functional with the correlation consistent polarized valence double-ζ (cc-pVDZ) base along with D3 dispersion correction,[29] which was applied here to study H-SiNCs using TURBOMOLE V7.0.[30] Thus, we calculated geometrical optimizations of H-SiNCs and afterward we analyzed the triplet-singlet stability of the Kohn−Sham (KS) wave function. Upon encountering instabilities, we removed the spatial-spin orbit degeneracy constraint using the open-shell unrestricted broken symmetry (UB) approach to reoptimize the geometry of the singlet state. In addition, we use the CASSCF method (as implemented in Gaussian09[31]) with a modest active space of 10 orbitals and 10 electrons to determine the multiconfigurational character, and to determine whether or not monoreferential wave functions are efficient to describe the H-SiNCs thus obtained. Lastly, from the optimized geometries, the nonresonance Raman spectra were calculated for both the singlet and triplet states of H-SiNCs.

The structural arrangement of the H-SiNC (n_z,n_a) under study is depicted in Figure 1(a). Here the units on the armchair and zigzag edges of the rectangular nanoclusters are represented by $n_a \in [1,9]$ and $n_z \in [1,7]$, respectively. We set N as the number of fused rings given by $n_z \times n_a = N$. A side view of the H-SiNC structure is given in Figure 1b. Following previous conventions made for graphene nanoribbons,[32] hydrogen atoms are used in our calculations to passivate the dangling bonds at the edges of silicene, as shown in Figure 1c. For H-SiNC(8,8), we obtain Si−Si bond lengths ranging from 2.221 to 2.294 Å, and a buckling of 0.362 Å to 0.617 Å, which are similar to previous results.[36,37]

To facilitate our understanding of the multiconfigurational character of the H-SiNCs (n_z,n_a) structure, we now mention some features regarding spin contamination and electron correlation. A spin-unrestricted wave function for a given spin state can be written as a linear combination of the pure-spin wave functions plus contributions from higher spin states, resulting in an expectation value for the $\hat{S}^2$ operator that exceeds the exact $S(S + 1)$ value, because the contaminants tend to have relatively large values of S. In particular, spin contamination for any single-determinant spin-unrestricted wave function can be evaluated using the following equation[33]

$$\langle \hat{S}^2 \rangle_{NI} = S(S+1) + N_\beta - \sum_i^{N_\alpha} \sum_j^{N_\beta} | \int d\mathbf{r} \phi_i^{\alpha *}(\mathbf{r}) \phi_j^{\beta}(\mathbf{r}) |^2 \quad (1)$$

where NI stands for a noninteracting system, $S = (N_\alpha - N_\beta)/2$ is the net spin of a H-SiNC structure, with N_i being the number of spin-up (α) and spin-down (β) electrons. Here ϕ_i^α and ϕ_j^β are the orbitals coming from the spin-unrestricted case. Then, if the ϕ_i^α and ϕ_j^β orbitals are orthogonal in the singlet $(S = 0)$ ground state, there will be no spin contamination, and the unrestricted wave function is identical to the restricted one. Using eq 1, we give in Table 1, the computed relative energies for the singlet and triplet states, and their respective spin squared expectation values, $\langle \hat{S}^2 \rangle_{NI}$. All values are reported in kcal per mol for the calculated states, and the relative energies from Table 1 are given with respect to their corresponding closed shell singlet state energy (S_0-RB3LYP). The systems in this table that only register zeros did not show a triplet $(S = 1)$ state instability in their closed shell state wave function. Therefore, calculations using the UB3LYP method were not pursued further. As seen from Table 1, the energies for the open-shell species, (S_0-UB3LYP) and (S_1-UB3LYP), are always lower than their corresponding RB3LYP energies for $N \geq 15$. This energy decrease could arise from different causes, for instance, the use of different orbitals for each electron allows the α and β electrons to be more spatially separated on average than in a RB3LYP wave function. Overlap of electron orbitals introduces some electron correlation,[34] and the mixing of higher spin states causes the energy to increase. So, when electron correlation is included, the deviation of $\langle \hat{S}^2 \rangle$ from $S(S + 1)$ is simply due to the mixing of higher spin states. Therefore, since UB3LYP introduces electron correlation to a certain extent, the values of $\langle \hat{S}^2 \rangle$ presented in Table 1 suggest the presence of higher spin states. The stability of the H-SiNCs

DOI: 10.1021/acs.jpclett.6b02773
J. Phys. Chem. Lett. 2017, 8, 615−620

Table 1. Relative Energies in kcal/mol of the Open Shell Triplet (S_1-UB3LYP) and the Open Shell Singlet (S_0-UB3LYP) States, Each Taken with Respect to S_0-RB3LYP[a]

H-SiNC (n_z,n_a)	N	S_1-UB3LYP	$\langle\hat{S}^2\rangle_{NI}$	S_0-UB3LYP	$\langle\hat{S}^2\rangle_{NI}$
(1,1)	1	0	0	0	0
(2,1)	2	0	0	0	0
(3,1)	3	0	0	0	0
(4,1)	4	8.696	2.06	−0.182	0.47
(5,1)	5	4.579	2.07	−1.418	0.92
(6,1)	6	1.717	2.08	−3.103	1.23
(7,1)	7	−0.306	2.09	−4.910	1.50
(2,2)	4	0.00	0.000	0.00	0
(3,2)	6	0.00	0.000	0.00	0
(4,2)	8	4.90	2.118	−0.97	0.81
(5,2)	10	0.81	2.135	−3.07	1.20
(6,2)	12	−2.09	2.162	−5.45	1.54
(7,2)	14	−4.18	2.222	−7.85	1.85
(3,3)	9	8.52	2.104	0.00	0.31
(4,3)	12	1.60	2.123	−2.08	1.08
(5,3)	15	−3.01	2.145	−5.33	1.40
(6,3)	18	−5.91	2.168	−8.38	1.69
(7,3)	21	−7.64	2.190	−11.20	2.11
(4,4)	16	−0.37	2.159	−2.99	1.22
(4,5)	20	−2.164	2.19	−3.976	1.32
(4,6)	24	−13.423	2.22	−14.723	1.38
(4,7)	28	−4.779	2.25	−5.718	1.41
(4,8)	32	−5.793	2.28	−6.462	1.41
(4,9)	36	−11.663	2.31	−12.154	1.43
(5,4)	20	−5.25	2.189	−6.88	1.48
(6,4)	24	−8.093	2.22	−10.197	1.85
(7,4)	28	−9.564	2.27	−13.185	2.31
(7,6)	42	−12.480	3.31	−16.003	2.61

[a]The corresponding $\langle\hat{S}^2\rangle_{NI}$ expectation values are also shown for various (n_z,n_a) silicene nanoclusters. The subscript NI here denotes a non-interacting system.

is examined by comparing the energies of the singlet and triplet states. From the results thus obtained, we can observe that the ground state is given by the singlet state for $n_z > n_a$. These results agree well with a previous study, which states that infinitely long zigzag silicene nanoclusters with a width index, n_z, of four or higher have a singlet ground state,[35] and each edge silicon atom has a finite local magnetic moment. Along the n_a direction, the energy difference between the singlet and triplet states become closer to zero for $n_a > n_z$. The closeness in energy between S_1-UB3LYP and S_0-UB3LYP states could indicate a transition from a S_0 to a S_1 state as n_a increases. However, the energy differences for $n_a > 6$ between the singlet and triplet states at the DFT level of calculation are not decisive because the results are within the accuracy limits of DFT.

Next we discuss the magnitude of the spin contamination $\langle\hat{S}^2\rangle$ for the singlet and triplet states. Figure 2a,b illustrates the deviation of the average $\langle\hat{S}^2\rangle$ values from their corresponding eigenvalues $S(S + 1)$ for $S = 0$ and $S = 1$ in the zigzag and armchair directions, respectively. Figure 3 shows that the $\langle\hat{S}^2\rangle$ values for the singlet state are the most seriously contaminated in comparison with the triplet state, indicating that the wave functions for the singlet state were severely contaminated with higher spin states. Furthermore, we observe that the spin contamination is more severe in the zigzag direction than in the armchair direction for the singlet state, with a ratio of $r = 9.3 \times n_z/n_a$ found from the two linear regressions. For the triplet

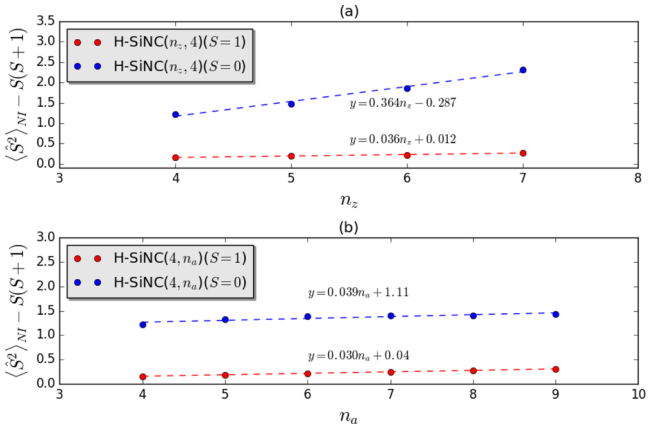

Figure 2. Deviation of the $\langle\hat{S}^2\rangle_{NI}$ values from $S(S + 1)$ as a function of the length of the ribbon in the (a) zigzag n_z and (b) armchair n_a direction, respectively. The results were taken from Table 1.

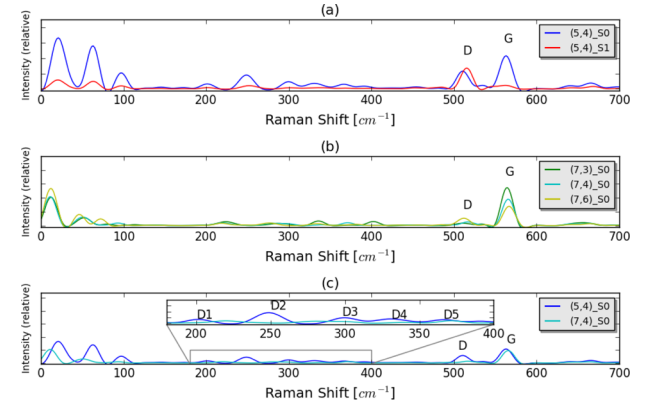

Figure 3. Rama spectra of different H-SiNCs obtained by convoluting the calculated vibrational spectrum with a uniform Gaussian broadening having a 10 cm^{-1} linewidth. (a) Raman spectrum for the triplet and singlet states of H-SiNC(5,4). (b) Raman spectrum of H-SiNC(7,n_a) as a function of n_a. (c) Raman spectrum of H-SiNC(n_z,4) as a function of n_z. The inset graph shows an expancion of panel c for the frequencies at around 200−400 cm^{-1}.

state, the spin contamination increases almost at the same rate for both zigzag and armchair directions with a ratio of $r = 1.2 \times n_z/n_a$, indicating that the predicted spin contamination is smaller in the triplet state than in the singlet state.

Due to the detection of higher spin states with the single-determinantal spin-unrestricted wave functions (see Table 1), we use multireferential first principals calculations, in this case, using the CASSCF (10,10) method with a G-31G(d) basis set. We were thus able to obtain energies for the different optimized multiplets, along with their respective configuration-interaction (CI) expansion coefficients for different configurations, and, consequently, we can obtain the most representative configurations (see Table 2). When the number of fused rings becomes large ($N \geq 12$), it appears that subsequent H-SiNCs are equally likely to have both triplet and singlet ground states, and this is represented physically by a very small energy difference between these states. However, when $n_a > n_z$, we observe that the triplet state is more stable than the singlet state as n_a increases, indicating that a phase transition from a singlet to a triplet ground state is likely. For $n_z > n_a$, the most stable state is the singlet state that can also be observed by revising the relative energies contained in Table 1.

DOI: 10.1021/acs.jpclett.6b02773
J. Phys. Chem. Lett. 2017, 8, 615−620

Table 2. Relative Energies [kcal/mol] and Greatest Squared CI Expansion Coefficients of Dominant Configurations Obtained by the CASSCF (10,10) Method for Both the $S = 0$ and $S = 1$ States[a]

		CI		
H-SiNC (n_z,n_a)	N	$S = 0$	$S = 1$	relative energy
(1,1)	1	0.78	0.56	33.019
(2,1)	2	0.65	0.49	24.304
(3,1)	3	0.67	0.65	16.151
(4,1)	4	0.60	0.63	9.474
(5,1)	5	0.47	0.61	4.430
(6,1)	6	0.48	0.65	3.438
(7,1)	7	0.54	0.65	5.447
(2,2)	4	0.74	0.58	24.742
(3,2)	6	0.71	0.68	20.088
(4,2)	8	0.64	0.69	5.362
(5,2)	10	0.66	0.72	9.956
(6,2)	12	0.40	0.70	0.547
(7,2)	14	0.42	0.73	0.455
(3,3)	9	0.71	0.68	20.066
(4,3)	12	0.67	0.70	2.261
(5,3)	15	0.36	0.67	0.277
(6,3)	18	0.38	0.72	0.235
(7,3)	21	0.33	0.65	0.138
(4,4)	16	0.71	0.70	6.567
(4,5)	20	0.39	0.74	0.099
(4,6)	24	0.36	0.69	0.134
(4,7)	28	0.35	0.69	−0.004
(4,8)	32	0.35	0.69	−0.008
(4,9)	36	0.38	0.75	−0.050
(5,4)	20	0.40	0.77	0.102
(6,4)	24	0.36	0.71	0.014
(7,4)	28	0.34	0.67	0.047
(7,6)	42	0.37	0.75	0.022

[a]The relative energies were calculated with respect to the singlet state.

On the other hand, it is possible to introduce a triplet ground state in the zigzag configuration by using asymmetric edges,[36,37] or using triangular shapes of silicene with hydrogen-passivate zigzag edges jointed by an odd-numbered Si chain.[38] It is well-known that as any chemical system's multiplicity increases, its multiconfigurational character becomes less relevant up to the point of being able to be successfully described by it is dominant configuration. Thus, for $N > 12$, the squared CI expansion coefficient for the $S = 1$ state exceeds 0.65, indicating the dominance of almost a single reference character for the $S = 1$ state. By contrast, for the $S = 0$ state, the squared CI expansion coefficient does not exceed 0.5, suggesting that the $S = 0$ state has a multireferential character. The dominant configurations obtained are 2222200000 and 2222$\alpha\alpha$0000 for the singlet and triplet states, respectively. The dominant configurations represent the electron distribution in the active orbitals; α represents the 1/2 spin state.

Using the calculated Raman spectra, we are now attempting to understand the multiconfigurational character of H-SiNCs(n_z,n_a) along the zigzag and armchair directions. To obtain the nonresonance Raman spectrum, we have carried out density functional calculations using UB3LYP with Dunning's correlation consistent basis[29] with the cc-pVDZ basis set. The interpretation of the silicene Raman spectrum is based on previously reported experimental data,[39] and the calculated phonon dispersion curve of silicene that is presented in the Yan et al. reference.[40] Moreover, we can deduce by analogy with graphene that the Raman-active modes of silicene are about one-third of the intensity of the respective resonant frequencies found for graphene for the optical phonon bands. In Figure 3a, we show the Raman spectrum for the H-SiNC(5,4)-S_0 and H-SiNC(5,4)-S_1 states, respectively. The Raman spectrum for the S_0 state presents two high intensity peaks around 563 and 512 cm^{-1}. The 563 cm^{-1} frequency is a doubly degenerate E_g (G peak) mode which corresponds to the in-plane transverse optical (iTO) branch and the in-plane longitudinal optical (iLO) phonon branches at the Γ point, which are both Raman active.[40] The other frequency 512 cm^{-1} represents the A_1 (D peak) mode that originates from the existence of the ribbon edge. However, it is interesting to mention that in graphene nanoribbons, only armchair edges are capable of elastically scattering charge carriers that give rise to the D peak.[41] The presence of this corresponding peak in graphene can also be related to the presence of structural defects.[42,43] Furthermore, we can notice a peak at around 665 cm^{-1} that is due to a vibration of the Si−H (1.5 Å) localized at the edge of the ribbons. The intensity of this peak decreases with increasing the width of the ribbon in the zigzag direction, which can then be used to determine the H-SiNCs' width experimentally. The origin of the frequencies around 200−400 cm^{-1} will be explained in the inset graph of Figure 3c. The Raman spectrum for the triplet state (S_1) simply shows an intense peak at around 516 cm^{-1} that corresponds to the symmetry-breaking D mode in silicene. In Figure 3b, we now explore the effect of increasing the number of fused rings in the n_a direction. As n_a increases the ratio of the relative intensity of the D and G peaks, $I(D)/I(G)$, increases, indicating that for $n_a > n_z$ the D peak will have a higher intensity. Now in Figure 3c, we keep n_a constant and change n_z showing that the intensity of the D peak decreases as n_z is increasing. However, the intensity of the G peak remains almost constant. The inset graph in Figure 3c shows that the D_1−D_5 peaks are attributed to electron inter- or intravalley scattering at zigzag and armchair edges.[42,44] Comparing Figure 3b,c, it is likely that the intensities of these peaks are associated with the armchair edges. Consequently, it is expected that more vibrational modes are induced for H-SiNCs when $n_a > n_z$. In the low frequency regions of all Raman spectra at around 20−100 cm^{-1}, we find other active peaks which correspond to the out-plane acoustic (ZA) phonons. This is because of the buckled structure of silicene, which breaks the reflection symmetry with respect to the atomic plane, thus generating strong ZA phonons. The intensity of these peaks decrease with increasing the width of the ribbon in the zigzag direction while these intensities remain constant for a fixed n_z as shown in the Figure 3b,c. Thus, according to the previous results shown in Tables 1 and 2, the triplet state can be observed for $n_a > n_z$, as is also shown in the Raman spectra for the H-SiNC(4,7) in the Supporting Information.

To obtain a more complete theoretical description of the ground states for these silicene type systems, we focused on one more property of interest, namely the HOMO−LUMO (H−L) gap (see Figure 4). This H−L energy gap provides a direct indicator of the material's band gap energy.[45]

The corresponding calculated H−L energy gaps have been plotted in Figure 4 as a function of the total number of fused rings (N) presented in Table 1 plus three new ones H-SiNC(7,7), H-SiNC(8,8), and H-SiNC(9,9), and the results are shown in Figure 4. From Figure 4, we note that the H−L energy gap decreases as N increases for the singlet state. This

DOI: 10.1021/acs.jpclett.6b02773
J. Phys. Chem. Lett. 2017, 8, 615−620

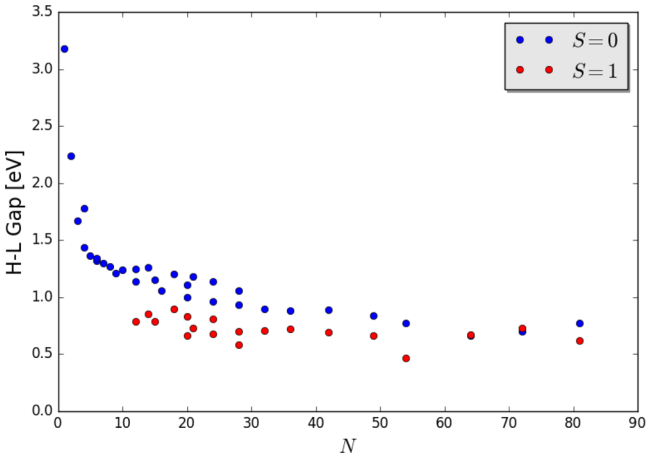

Figure 4. H−L gap in eV for H-SiNCs as a function of the number of fused rings N.

decreasing is rapid at first for $N < 10$ and more slow thereafter. A similar trend has been reported for carbon clusters with different diameters.[46] We can expect that for $N < 10$, quantum effects become important, so a large energy gap may be expected. Additionally for $N < 10$, we observe that the ground state is simply given by the singlet state. The H−L energy gaps for the triplet state are lower in energy than for the singlet state, indicating that the H-SiNCs in the armchair direction shows lower band gaps since the triplet state is more stable for $n_a > n_z$ as also shown in Table 2. In addition, we observe that the band gaps of both singlet and triplet states are higher than 0.4 eV which is very crucial for the application of silicene in nanoelectronics. We note that for $N = 64$, the H−L gaps for the singlet and triplet states become almost degenerate, and approach the degeneracy in the limit $N \rightarrow \infty$. This argument suggests that there might be a dramatic reduction of the H−L gap of silicene as $N \rightarrow \infty$, and its electronic properties could become similar to those of pure graphene such as a high residual carrier density.[11]

In summary, using first-principles calculations, we show that the singlet ground state of H-SiNCs becomes multiconfigurational upon increasing the size of the system, meaning that one determinant first principals methods may become inefficient for its description. Insight from the spin contamination provides good reason to believe that states with higher multiplicity may become relevant as the width of the rectangular nanocluster increases. Depending on whether the rectangular nanocluster edges are along armchair or zigzag directions, the ground state can be a singlet state (antiferromagnetic) for $n_z > n_a$, or a triplet state (ferromagnetic or paramagnetic) for $n_a > n_z$. The calculated Raman spectra for the different multiplicities allow us to detect a D peak that is associated with the armchair edges with a triplet ground state. Additionally, we show that the H−L gap decreases for both the singlet and triplet states; however, in comparing the singlet and triplet cases containing the same number of Si and H atoms, the H−L gap decays faster for the singlet state. The decay of the H−L gap in the singlet case shows that the H−L gap diminishes for a very large N as expected. Therefore, we found that silicene itself could be a material with a zero band gap for a very large system as previously reported, while a finite system of silicene is expected to exhibit a nonzero H−L gap, which depends on the number of fused rings N and the topology of the edges of the rectangular silicene nanoclusters, i.e. armchair versus zigzag. Furthermore, such rectangular silicene nanocluster can exhibit a triplet state for $n_a > n_z$. Study of the H−L gap and its tunability as a function of the rectangular nanocluster length could make silicene a good candidate for future nanotechnology applications.

■ ASSOCIATED CONTENT

Supporting Information

The Supporting Information is available free of charge on the ACS Publications website at DOI: 10.1021/acs.jpclett.6b02773.

Detailed discussion of the theoretical methodology used and a table of additional computational data showing the stability of the reported results with respect to the geometry optimization techniques and the basis set choice, as well as the Raman spectrum for the H-SiNC (4,7) structure along with its spin density distribution (PDF)

■ AUTHOR INFORMATION

Corresponding Author

*E-mail: fomine@unam.mx.

ORCID

Ricardo Pablo-Pedro: 0000-0003-4659-1996

Hector Lopez-Rios: 0000-0002-8775-8046

Author Contributions

‖These authors contributed equally. The manuscript was written through contributions of all authors. All authors have given approval to the final version of the manuscript.

Notes

The authors declare no competing financial interest.

■ ACKNOWLEDGMENTS

H.L.R. gratefully acknowledges the Consejo Nacional de Ciencia y Tecnologia (CONACyT) for the graduate fellowship (291062). M.S.D. and R.P.-P. acknowledge the King Abdullah University of Science and Technology for support under contract (OSR- 2015-CRG4-2634). H.L.R. and S.F. also acknowledge the financial support from DGPA (Grant IN100215).

■ ABBREVIATIONS

DFT, density functional theory; CASSCF, complete active space self-consistent field; H-SiNRs, silicene nanoribbons with hydrogen passivated edges; CI, configuration interaction; H-L, HOMO−LUMO

■ REFERENCES

(1) Takeda, K.; Shiraishi, K. Theoretical Possibility of Stage Corrugation in Si and Ge Analogs of Graphite. *Phys. Rev. B: Condens. Matter Mater. Phys.* **1994**, *50*, 14916−14922.

(2) Cahangirov, S.; Topsakal, M.; Aktürk, E.; Şahin, H.; Ciraci, S. Two- and One-Dimensional Honeycomb Structures of Silicon and Germanium. *Phys. Rev. Lett.* **2009**, *102*, 236804.

(3) Sahaf, H.; Masson, L.; Leándri, C.; Aufray, B.; Le Lay, G.; Ronci, F. Formation of a One-Dimensional Grating at the Molecular Scale by Self-Assembly of Straight Silicon Nanowires. *Appl. Phys. Lett.* **2007**, *90*, 263110.

(4) De Padova, P.; Quaresima, C.; Olivieri, B.; Perfetti, P.; Le Lay, G. sp_2-like Hybridization of Silicon Valence Orbitals in Silicene Nanoribbons. *Appl. Phys. Lett.* **2011**, *98*, 081909.

DOI: 10.1021/acs.jpclett.6b02773
J. Phys. Chem. Lett. 2017, 8, 615−620

(5) Fleurence, A.; Friedlein, R.; Ozaki, T.; Kawai, H.; Wang, Y.; Yamada-Takamura, Y. Experimental Evidence for Epitaxial Silicene on Diboride Thin Films. *Phys. Rev. Lett.* **2012**, *108*, 245501.
(6) Zhang, X.; Xie, H.; Hu, M.; Bao, H.; Yue, S.; Qin, G.; Su, G. Thermal Conductivity of Silicene Calculated Using an Optimized Stillinger-Weber Potential. *Phys. Rev. B: Condens. Matter Mater. Phys.* **2014**, *89*, 054310.
(7) Liu, C. C.; Feng, W.; Yao, Y. Quantum Spin Hall Effect in Silicene and Two-Dimensional Germanium. *Phys. Rev. Lett.* **2011**, *107*, 076802.
(8) Feng, B.; Ding, Z.; Meng, S.; Yao, Y.; He, X.; Cheng, P.; Chen, L.; Wu, K. Evidence of Silicene in Honeycomb Structures of Silicon on Ag(111). *Nano Lett.* **2012**, *12*, 3507−3511.
(9) Quhe, R.; Yuan, Y.; Zheng, J.; Wang, Y.; Ni, Z.; Shi, J.; Yu, D.; Yang, J.; Lu, J. Does the Dirac Cone Exist in Silicene on Metal Substrates? *Sci. Rep.* **2014**, *4*, 1−8.
(10) Kara, A.; Enriquez, H.; Seitsonen, A. P.; Lew Yan Voon, L. C.; Vizzini, S.; Aufray, B.; Oughaddou, H. A Review on Silicene - New Candidate for Electronics. *Surf. Sci. Rep.* **2012**, *67*, 1−18.
(11) Tao, L.; Cinquanta, E.; Chiappe, D.; Grazianetti, C.; Fanciulli, M.; Dubey, M.; Molle, A.; Akinwande, D. Silicene Field-Effect Transistors Operating at Room Temperature. *Nat. Nanotechnol.* **2015**, *10*, 227−231.
(12) Guzmán-Verri, G. G.; Lew Yan Voon, L. C. Electronic Structure of Silicon-Based Nanostructures. *Phys. Rev. B: Condens. Matter Mater. Phys.* **2007**, *76*, 075131.
(13) Guo, Z. X.; Furuya, S.; Iwata, J. I.; Oshiyama, A. Absence and Presence of Dirac Electrons in Silicene on Substrates. *Phys. Rev. B: Condens. Matter Mater. Phys.* **2013**, *87*, 235435.
(14) Ganesh, P.; Kim, J.; Park, C.; Yoon, M.; Reboredo, F. A.; Kent, P. R. C. Binding and Diffusion of Lithium in Graphite: Quantum Monte Carlo Benchmarks and Validation of Van Der Waals Density Functional Methods. *J. Chem. Theory Comput.* **2014**, *10*, 5318−5323.
(15) Williamson, A. J.; Hood, R. Q.; Needs, R. J.; Rajagopal, G. Diffusion Quantum Monte Carlo Calculations of the Excited States of Silicon. *Phys. Rev. B: Condens. Matter Mater. Phys.* **1998**, *57*, 12140−12144.
(16) Liu, C. C.; Jiang, H.; Yao, Y. Low-Energy Effective Hamiltonian Involving Spin-Orbit Coupling in Silicene and Two-Dimensional Germanium and Tin. *Phys. Rev. B: Condens. Matter Mater. Phys.* **2011**, *84*, 195430.
(17) Ni, Z.; Liu, Q.; Tang, K.; Zheng, J.; Zhou, J.; Qin, R.; Gao, Z.; Yu, D.; Lu, J. Tunable Bandgap in Silicene and Germanene. *Nano Lett.* **2012**, *12*, 113−118.
(18) Köhler, A.; Beljonne, D. The Singlet−Triplet Exchange Energy in Conjugated Polymers. *Adv. Funct. Mater.* **2004**, *14*, 11−18.
(19) Plasser, F.; Pašalić, H.; Gerzabek, M. H.; Libisch, F.; Reiter, R.; Burgdörfer, J.; Müller, T.; Shepard, R.; Lischka, H. The Multiradical Character of One- and Two-Dimensional Graphene Nanoribbons. *Angew. Chem., Int. Ed.* **2013**, *52*, 2581−2584.
(20) Torres, A. E.; Guadarrama, P.; Fomine, S. Multiconfigurational Character of the Ground States of Polycyclic Aromatic Hydrocarbons. A Systematic Study. *J. Mol. Model.* **2014**, *20*, 1−7.
(21) Roos, B. O.; Taylor, P. R.; Siegbahn, P. E. M. A Complete Active Space SCF Method (CASSCF) Using a Density Matrix Formulated Super-CI Approach. *Chem. Phys.* **1980**, *48*, 157−173.
(22) Schlegel, H. B. Potential Energy Curves Using Unrestricted Mo/ller−Plesset Perturbation Theory with Spin Annihilation. *J. Chem. Phys.* **1986**, *84*, 4530−4534.
(23) Huzak, M.; Deleuze, M. S.; Hajgató, B. Half-Metallicity and Spin-Contamination of the Electronic Ground State of Graphene Nanoribbons and Related Systems: An Impossible Compromise? *J. Chem. Phys.* **2011**, *135*, 104704.
(24) Ouyang, F. P.; Peng, S. L.; Liu, Z. F.; Liu, Z. Bandgap Opening in Graphene Antidot Lattices: The Missing Half. *ACS Nano* **2011**, *5*, 4023−4030.
(25) Wang, J. Y.; Huang, H. Q.; Duan, W. H.; Liu, Z. Identifying Dirac Cones in Carbon Allotropes with Square Symmetry. *J. Chem. Phys.* **2013**, *139*, 184701.
(26) Li, W. F.; Guo, M.; Zhang, G.; Zhang, Y. W. Gapless MoS2 Allotrope Possessing both Massless Dirac and Heavy Fermions. *Phys. Rev. B: Condens. Matter Mater. Phys.* **2014**, *89*, 205402.
(27) Green, D.; Santos, L.; Chamon, C. Isolated Flat Bands and Spin-1 Conical Bands in Two-Dimensional Lattices. *Phys. Rev. B: Condens. Matter Mater. Phys.* **2010**, *82*, 075104.
(28) Linder, J.; Robinson, J. W. A. Superconducting Spintronics. *Nat. Phys.* **2015**, *11*, 307−315.
(29) Grimme, S.; Antony, J.; Ehrlich, S.; Krieg, H. A Consistent and Accurate ab Initio Parametrization of Density Functional Dispersion Correction (DFT-D) for the 94 Elements H-Pu. *J. Chem. Phys.* **2010**, *132*, 154104.
(30) TURBOMOLE V7.0 2015, A Development of University of Karlsruhe and Forschungszentrum Karlsruhe GmbH, 1989−2007, TURBOMOLE GmbH, since 2007. Available from http://www.turbomole.com.
(31) Frisch, M. J.; Trucks, G. W.; Schlegel, H. B.; Scuseria, G. E.; Robb, M. A.; Cheeseman, J. R.; Scalmani, G.; Barone, V.; Mennucci, B.; Petersson, G. A. et al., *Gaussian 09*, revision D.01; Gaussian Inc.: Wallingford, CT, 2013.
(32) Son, Y. W.; Cohen, M. L.; Louie, S. G. Energy Gaps in Graphene Nanoribbons. *Phys. Rev. Lett.* **2006**, *97*, 216803.
(33) Cohen, A. J.; Tozer, D. J.; Handy, N. C. *J.* Evaluation of $\langle S^2 \rangle$ in Density Functional Theory. *J. Chem. Phys.* **2007**, *126*, 214104.
(34) Knowles, P. J.; Handy, N. C. Projected Unrestricted Mo/ller−Plesset Second-Order Energies. *J. Chem. Phys.* **1988**, *88*, 6991−6998.
(35) Ding, Y.; Ni, J. Electronic Structures of Silicon Nanoribbons. *Appl. Phys. Lett.* **2009**, *95*, 083115.
(36) Ding, Y.; Wang, Y. Electronic Structures of Zigzag Silicene Nanoribbons with Asymmetric sp^2-sp^3. *Appl. Phys. Lett.* **2013**, *102*, 143115.
(37) Zberecki, K.; Swirkowicz, R.; Wierzbicki, M.; Barnas, J. Enhanced Thermoelectric Efficiency in Ferromagnetic Silicene Nanoribbons Terminated with Hydrogen Atoms. *Phys. Chem. Chem. Phys.* **2014**, *16*, 12900−12908.
(38) Luan, H-x.; Zhang, C-w.; Li, F.; Wang, Pj. Electronic and Magnetic Properties of Silicene Nanoflakes by First-Principles Calculations. *Phys. Lett. A* **2013**, *377*, 2792−2795.
(39) Zhuang, J.; Xu, X.; Du, Y.; Wu, K.; Chen, L.; Hao, W.; Wang, J.; Yeoh, W. K.; Wang, X.; Dou, S. X. Investigation of Electron-Phonon Coupling in Epitaxial Silicene by *in Situ* Raman Spectroscopy. *Phys. Rev. B: Condens. Matter Mater. Phys.* **2015**, *91*, 161409.
(40) Yan, J. A.; Stein, T.; Schaefer, D. M.; Wang, X. Q.; Chou, M. Y. Electron-Phonon Coupling in Two-Dimensional Silicene and Germanene. *Phys. Rev. B: Condens. Matter Mater. Phys.* **2013**, *88*, 121403.
(41) Cançado, L. G.; Pimenta, M. A.; Neves, B. R. A.; Dantas, M. S. S.; Jorio, A. Influence of the Atomic Structure on the Raman Spectra of Graphite Edges. *Phys. Rev. Lett.* **2004**, *93*, 247401.
(42) Pimenta, M. A.; Dresselhaus, G.; Dresselhaus, M. S.; Cançado, L. G.; Jorio, A.; Saito, R. Studying Disorder in Graphite-Based Systems by Raman Spectroscopy. *Phys. Chem. Chem. Phys.* **2007**, *9*, 1276−1290.
(43) Ferrari, A. C.; Meyer, J. C.; Scardaci, V.; Casiraghi, C.; Lazzeri, M.; Mauri, F.; Piscanec, S.; Jiang, D.; Novoselov, K. S.; Roth, S.; Geim, A. K. Raman Spectrum of Graphene and Graphene Layers. *Phys. Rev. Lett.* **2006**, *97*, 187401.
(44) Casiraghi, C.; Hartschuh, A.; Qian, H.; Piscanec, S.; Georgi, C.; Fasoli, A.; Novoselov, K. S.; Basko, D. M.; Ferrari, A. C. Raman Spectroscopy of Graphene Edges. *Nano Lett.* **2009**, *9*, 1433−1441.
(45) Muscat, J.; Wander, A.; Harrison, N. M. On the Prediction of Band Gaps from Hybrid Functional Theory. *Chem. Phys. Lett.* **2001**, *342*, 397−401.
(46) Lonfat, M.; Marsen, B.; Sattler, K. The Energy Gap of Carbon Cluster Studied by Scanning Tunneling Spectroscopy. *Chem. Phys. Lett.* **1999**, *313*, 539−543.

DOI: 10.1021/acs.jpclett.6b02773
J. Phys. Chem. Lett. 2017, 8, 615−620